JOURNAL OF AIRCRAFT
Vol. 31, No. 4, July–Aug. 1994

Quantitative Study of Unsteady Compressible Flow on an Oscillating Airfoil

L. W. Carr*
NASA Ames Research Center, Moffett Field, California 94035
M. S. Chandrasekhara†
Naval Postgraduate School, Monterey, California 93943
and
N. J. Brock‡
Aerometrics, Sunnyvale, California 94086

Real-time interferometric measurements of the flow near the leading edge of an oscillating airfoil offer detailed experimental quantification of the locally compressible flowfield that surrounds an oscillating airfoil at moderate subsonic Mach numbers. Interferograms obtained by a specially adapted real-time point-diffraction interferometry technique have revealed some important characteristics of this complex, and very rapidly varying, locally supersonic flow. Instantaneous pressure distributions determined from these interferograms document the effect of unsteadiness on the leading-edge flow environment.

Nomenclature

C_p = pressure coefficient
c = airfoil chord
f = frequency of oscillation, Hz
k = reduced frequency, $(\pi fc/U_\infty)$
L = test section span
M_∞ = freestream Mach number
n = refractive index
n_{ref} = refractive index at reference conditions
n_0 = refractive index at atmospheric conditions
U_∞ = freestream velocity
x = chordwise distance
z = distance along airfoil span
α = angle of attack
$\overline{\Delta PL}$ = average path length difference
ε = fringe number
λ_0 = wavelength of the laser
ρ = density
ρ_r = density at reference conditions
ρ_0 = density at atmospheric conditions
ϕ = phase angle of oscillation
ω = circular frequency, rad/s

I. Introduction

QUANTIFICATION of the complex unsteady flowfield associated with dynamic stall continues to be of considerable importance. The present inability to control and/or modify the dynamic stall phenomenon has limited the speed and agility of helicopters, and has prevented the use of unsteady lift for improvement of aircraft agility and maneuverability. Many studies of this aerodynamic phenomenon have been performed; see Carr[1] for a summary. Recent studies using the facility described in this article have shown that compressibility effects can and do play a significant role in the development of the unsteady flowfield on rapidly pitching airfoils.[2,3] However, truly quantitative, simultaneous documentation of the compressible flowfield on and away from the surface of the airfoil has not been available up to the present time. Surface measurements have been made in the past,[4,5] but knowledge of the flow behavior away from the surface is also necessary before control and/or modification of the stall process can be implemented. The work presented in this article supplies some of this information.

II. Facility and Instrumentation

The present study was performed in the Compressible Dynamic Stall Facility (CDSF) at the NASA Ames Research Center Fluid Mechanics Laboratory (FML). The CDSF is specifically designed for the study of dynamic stall over a range of Mach numbers, using nonintrusive optical flow diagnostic techniques. It is operated as a part of the in-draft tunnel complex at the FML.[6] The CDSF is unique in that the airfoil is supported between two 2.54-cm-thick optical quality glass windows by pins that are smaller than the local airfoil thickness. Thus, the entire flowfield, including the airfoil surface, can be viewed unobstructed by any support mechanism. This permits the study of the flow at the surface near the leading edge, where the dynamic stall vortex forms, as well as the flowfield away from the airfoil. Details of the research findings from earlier work in this facility can be found in Refs. 2, 3, and 6. The present tests were performed for $\alpha = 10$ deg $-$ 10-deg sin ωt, $0.28 \leq M_\infty \leq 0.47$, and $0.0 \leq k \leq 0.10$.

III. Flow Visualization

A. Point Diffraction Interferometry Technique

Point diffraction interferometry (PDI) is a technique that permits recording of real-time interferograms of a flow.[7–10] The PDI technique utilizes the ability of a point discontinuity (in the form of a pinhole or clear aperture), located at the

Presented as Paper 91-1683 at the AIAA 22nd Fluid Dynamics, Plasma Dynamics and Lasers Conference, Honolulu, HI, June 24–26, 1991; received Jan. 3, 1993; revision received Oct. 8, 1993; accepted for publication Oct. 11, 1993.

*Group Leader, Unsteady Viscous Flows, Aeroflightdynamics Directorate, U.S. Army ATCOM and Fluid Mechanics Laboratory Branch, M/S 260-1. Member AIAA.
†Associate Director and Research Associate Professor, Navy-NASA Joint Institute of Aeronautics, Department of Aeronautics and Astronautics. Associate Fellow AIAA.
‡Scientist; currently Scientist at Metrolaser, 18006 Skypark Circle, Irvine, California 92714.

image of a point source (Fourier transform plane), to diffract a portion of the incident light into a spherical reference wave front. Light passing through the flowfield under investigation is focused onto a sheet of partially transmitting material containing the pinhole. A portion of this light is diffracted by the pinhole creating a reference wavefront. The resulting reference wavefront then interferes with the undiffracted light that passes around the pinhole. The interference fringes that are produced by this method provide contours of optical path difference caused by density variations in the flowfield. Since the mathematical derivations associated with PDI are well-documented in the referenced papers,[7-9] this article will only address the physical implementation.

B. Implementation

In the present application, the primary optics of an existing schlieren system are used, with a pulsed Nd-YAG laser replacing the conventional spark as the light source, and the above-mentioned point diffractor replacing the usual knife edge.[11] Laser light is expanded to fill a portion of the first schlieren mirror, where it reflects through the test section and finally is refocused onto the diffracting plate by the second schlieren mirror. A camera placed at the image plane of the flowfield records the interference pattern.

Diffracting pinholes were made by placing a photographic emulsion precisely at the focus of the second schlieren mirror. With no flow in the test section, laser energy was increased until a pinhole was burned through the emulsion. Once the pinhole was made, it was left in place, and the laser energy was decreased to a level that adequately exposed the camera film without destroying the pinhole.

The photographic plate (Agfa 8E75) used to make the diffracting pinhole was processed with a weak developer and then exposed uniformly with light in order to make the emulsion darker (plates with emulsions darkened to optical densities of approximately one were used for the flow situations encountered in this test); no other processing was required. The increased absorption is necessary to attenuate the light passing around the pinhole (object wave) to a level equal in intensity to the light that diffracts from the pinhole (reference wave), thereby maximizing fringe contrast. The optical density necessary depends on how much the light is disturbed as it passes through the test section. An increase in disturbance (e.g., those associated with the stronger density gradients that appear at high angles of attack) results in an increase in the diameter of the focused beam at the pinhole, and a decrease in the intensity of the light diffracting through the pinhole, thereby requiring a higher optical density for the PDI plate for optimum fringe contrast.

IV. Flow Characteristics

A. General Flow Characteristics

The interferogram presented in Fig. 1 shows in detail the developing compressible flowfield around the leading edge of the pitching airfoil just prior to the initiation of dynamic stall. This figure presents the flow at $\alpha = 10.0$ deg for $M_\infty = 0.30$, and $k = 0.075$, and shows several characteristics of the unsteady flowfield. For example, the stagnation point on the lower surface is easily discernible, at the center of the smallest closed contour of constant density. It should also be noted that this stagnation point quantifies the density field for the complete interferogram, since the total pressure of the surrounding flow is attained at the stagnation point on the airfoil. This allows quantification of the fringe-related Mach contours for the complete flowfield around the airfoil.

The flow accelerates as it progresses around the leading edge, as represented by the closely spaced fringes emanating from the leading-edge region. As the flow continues to move around the airfoil, it continues to accelerate, until the surface curvature decreases, where a plateau appears in the density contours. This region shows very little longitudinal gradient,

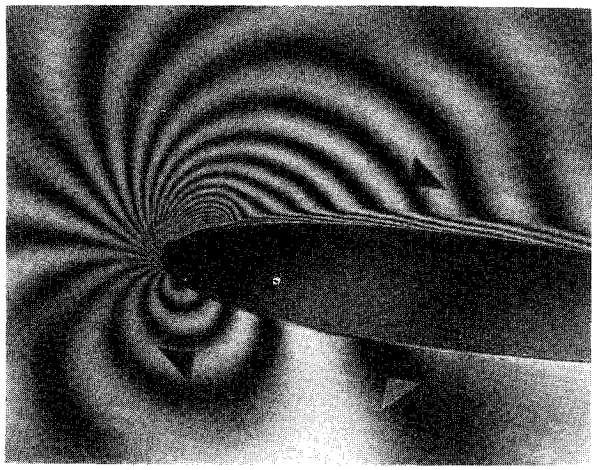

Fig. 1 PDI image of an oscillating airfoil flowfield, $\alpha = 10.0$ deg, $k = 0.075$, $M_\infty = 0.30$.

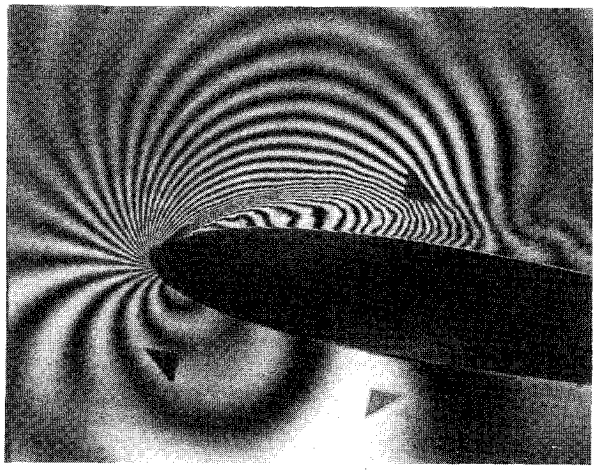

Fig. 2 PDI image of the dynamic stall vortex on an oscillating airfoil, $\alpha = 13.6$ deg, $k = 0.075$, $M_\infty = 0.30$.

and in fact shows the constant-density contours to be almost parallel to the surface of the airfoil in this region. Further down the airfoil, these contours abruptly turn toward the surface. The contour lines outside this region curve more gradually toward the surface, and can be seen to define the boundary layer over the remaining portion of the airfoil surface. The shape of the fringe contours inside this region suggest the presence of a laminar separation bubble. The conditions of the present experiment (NACA 0012 airfoil, $Re = 6 \times 10^5$) are appropriate for a laminar bubble to appear near the leading edge of the airfoil. The formation of the laminar separation bubble has also been confirmed by laser Doppler velocimetry (LDV) studies performed in the CDSF[12,13] for $M_\infty = 0.3$, $k = 0.05$. The angles of attack at which the bubble forms $\alpha = 6$ deg, and opens, $\alpha = 14$ deg, are nearly the same as determined by both LDV and PDI.

Figure 2 presents the flowfield for $\alpha = 13.6$ deg. In this figure, the dynamic stall vortex has formed, and the density field can be seen to be dramatically altered. The most significant change in the character of the flow appears on the upper surface near the leading edge. There is now a clearly defined shear layer leaving the leading edge; this shear layer shows very strong gradients. Also, the flowfield associated with the dynamic stall vortex shows a strong longitudinal gradient as depicted by the vertical density contours appearing along the upper surface near 25% chord. This figure presents a quantitative image of the Mach number environment of the airfoil at this point in the oscillation, and can be used directly to evaluate the accuracy of computational models of the dynamic stall process.

B. Character of Dynamic Stall Onset

An interferogram obtained at $\alpha = 12.4$ deg (at the onset of dynamic stall) is presented in Fig. 3. Here, the fringe pattern is similar to that observed in Fig. 1 near the leading edge, and near the beginning of the bubble, but the downstream edge of the bubble now has fringes extending downstream, parallel to the surface, in contrast to the sharp turning toward the surface seen in Fig. 1. In fact, the first indication of breakdown of the flow leading to dynamic stall appears as this change of the fringe contours at the downstream end of the bubble, suggesting a failure of the turbulent flow to reattach. Finally, Fig. 4, at $\alpha = 13.07$ deg, shows the initial development of the dynamic stall vortex, which develops from the bubble shown in Fig. 3. The fringes near the surface downstream of the bubble have now turned sharply toward the surface. Since each fringe indicates a specific density, this image shows that there is now a region of low density, and therefore, low pressure, extending along the airfoil surface. This also affects the flow away from the surface, as can be seen in the outer fringes that also curve around this low-pressure region. This pattern of opening of the laminar separation bubble was detected throughout the frequency and Mach number range explored to date, and suggests that the dynamic stall process in the present experiment is either caused by a breakdown of the laminar separation bubble, or by events occurring within the bubble that have yet to be documented. This re-emphasizes that dynamic stall can be caused by a wide range of fluid physics while resulting in very similar global flow behavior. Future tests will investigate various types of leading-edge, boundary-layer transition generators, so that CDSF airfoil tests can fully reproduce the various types of leading- and trailing-edge dynamic stall conditions observed in full-scale tests.

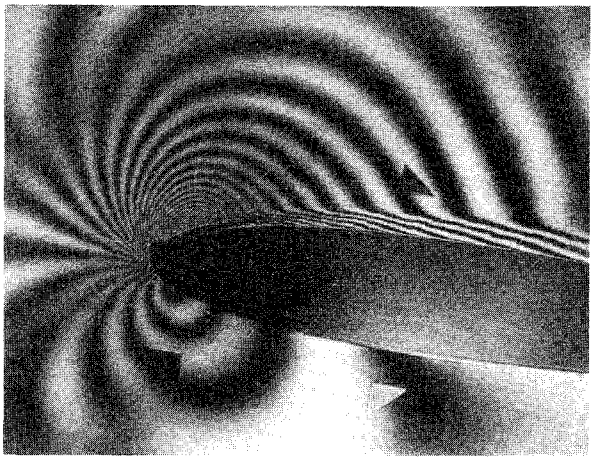

Fig. 3 PDI image of the opening of the laminar separation bubble; $M_\infty = 0.30$, $k = 0.075$, $\alpha = 12.4$ deg.

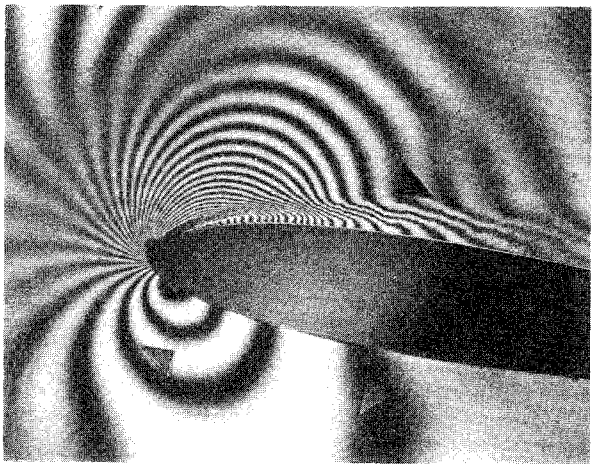

Fig. 4 PDI image of the initial phase of dynamic stall vortex at $M_\infty = 0.30$, $k = 0.075$, $\alpha = 13.07$ deg.

C. Influence of Reduced Frequency

The effect of reduced frequency on flow development over the airfoil can be seen in Fig. 5. In this figure, the influence of unsteadiness is shown at four angles of attack. The top row of photographs shows the effect of frequency on the flow at $\alpha = 8$ deg. The presence of the laminar separation bubble can be seen at $k = 0.0$. At this angle of attack, the bubble is suppressed by airfoil oscillation; the flow at $k = 0.075$ and 0.10 do not show the bubble—the contours are similar to those at lower angle of attack (not shown). At $\alpha = 10$ deg (second row of photographs) the bubble is present at all frequencies. At $\alpha = 12$ deg (third row of photographs), the first indication that oscillation delays stall is observed: the steady flow has stalled, but even low level oscillation ($k = 0.025$) suppresses separation and re-establishes fully attached flow. At $\alpha = 14$ deg, this effect is even more clearly discernible: as the frequency increased above $k = 0.05$, the stall is suppressed further, whereas a dynamic stall vortex appears at lower reduced frequencies. The development of this vortex is progressively delayed as the frequency is increased. Thus, as the frequency reaches $k = 0.10$, the dynamic stall process is just beginning at an angle 2 deg higher than the angle at which the airfoil completely stalls in steady flow.

D. Effect of Mach Number

The effect of Mach number at $k = 0.05$ can be seen in Fig. 6. At $\alpha = 6$ deg (first row of photographs), the flow varies smoothly from the stagnation point to the trailing edge (out of the view of the photograph). As the Mach number is increased, a progressive increase in the fringe count is apparent, as can be expected, due to the greater density variations that occur at the higher Mach numbers. At $\alpha = 8$ deg (second row), the presence of the laminar separation bubble is observed. This bubble is not measurably altered as the Mach number is increased, except for the increase in fringe density reflecting the increase in Mach number. At $\alpha = 10$ deg (third row), some very interesting flow physics can be seen in the laminar separation bubble. As the Mach number is increased to $M_\infty = 0.42$, vertical lines appear in the bubble. These vertical lines can be seen more clearly at $M_\infty = 0.47$, where the fringes are seen to bend discontinuously as they pass through the vertical lines. The local Mach number obtained by fringe counting was found to be 1.0–1.1; thus, the local flow is slightly supersonic. The multiple shock waves seen are a feature of transonic laminar flow over mildly curving surfaces; this condition of multiple shocks has been observed in other experiments.[14,15] It is interesting that the current study shows the phenomenon to be present even in unsteady flows, where the events occur at different angles of attack depending on the reduced frequency.

At $\alpha = 12$ deg (fourth row), the influence of compressibility on the dynamic stall process is quite evident. The flow on the airfoil at $M_\infty = 0.28$ is clearly attached. However, at $M_\infty = 0.33$, the dynamic stall process has begun, and at $M_\infty = 0.38$ the dynamic stall vortex is evident. At $M_\infty = 0.42$, the vortex is already past $x/c = 0.25$, and at $M_\infty = 0.47$, the vortex is already out of the field of view. These photographs graphically show that the dynamic stall inception angle is a direct function of the Mach number.

V. Quantitative Analysis of the Unsteady Flowfield

A. Mach Contours

The interferograms presented in this study offer quantitative information concerning the Mach contours of the flow under investigation.

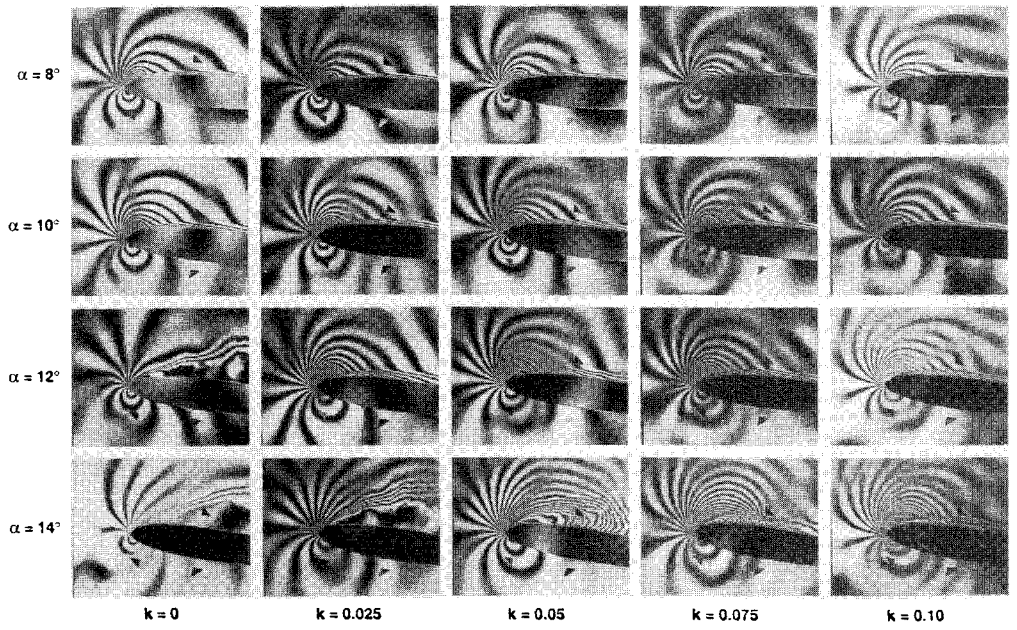

Fig. 5 Effect of frequency on dynamic stall development, $M_\infty = 0.30$, $\alpha = 10$ deg $-$ 10 deg sin ωt (as indicated).

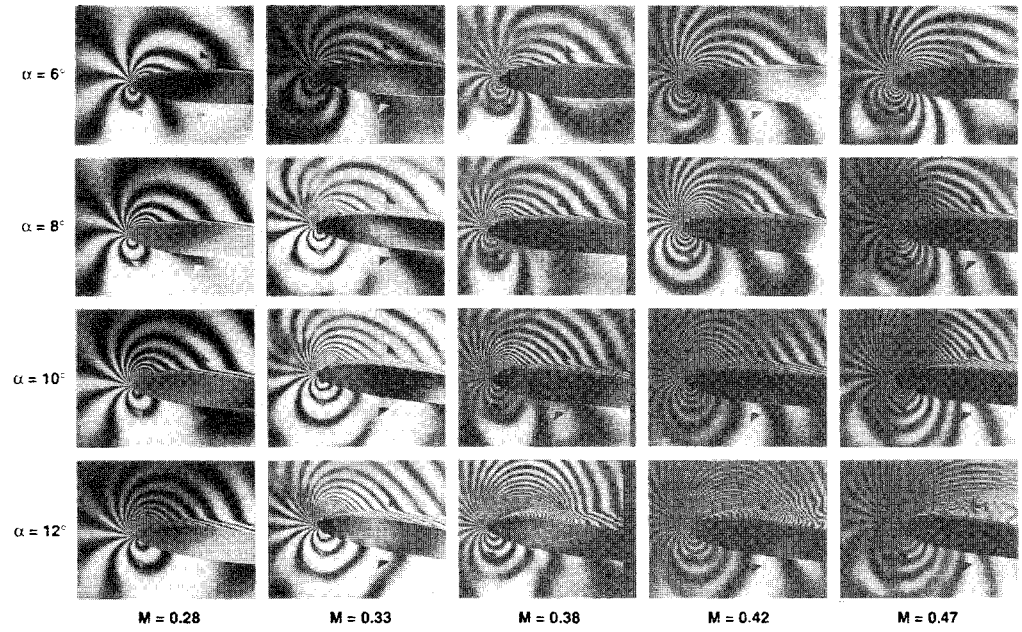

Fig. 6 Effect of Mach number on dynamic stall development, $k = 0.05$, $\alpha = 10$ deg $-$ 10 deg sin ωt (as indicated).

For a standard interferometer, $\overline{\Delta PL}$ due to density (or phase) changes can be related to ε as

$$\varepsilon = \frac{\overline{\Delta PL}}{\lambda_0} = \frac{1}{\lambda_0}\int (n - n_{\text{ref}})\, dz$$

where n is the refractive index in the signal beam.

For a two-dimensional flow, the above equation can be simplified to

$$\varepsilon = (n - n_{\text{ref}})(L/\lambda_0)$$

If ε is an integer, then the fringe is bright; and if it is a half integer, the fringe is dark. Using the Gladstone-Dale equation and the perfect gas equation, this equation can be reduced to[16]

$$\rho - \rho_r = \left(\frac{\lambda_0}{n_0 - 1}\right)\left(\frac{\varepsilon\rho}{L}\right) = A\varepsilon$$

Since $\lambda_0 = 532$ nm, $L = 25$ cm, $(n_0 - 1) = 2.733 \times 10^{-4}$ (from Goldstein[16]), and $\rho_0 = 1.21$ kg/m^3, the constant A can be determined. For the specific case of the present experiments

$$\rho - \rho_0 = 0.009421\varepsilon$$

or

$$\frac{\rho}{\rho_0} = \frac{\rho_r}{\rho_0} + \frac{A\varepsilon}{\rho_0}$$

Since (ρ_r/ρ_0) is a function of the freestream Mach number only, (ρ/ρ_0) can be determined by knowing the fringe number. Note, that in this method a positive fringe number represents deceleration, and vice versa.

B. Digitization of Interferograms

In order to make full use of the quantification that interferometry offers, the photographs containing the interfero-

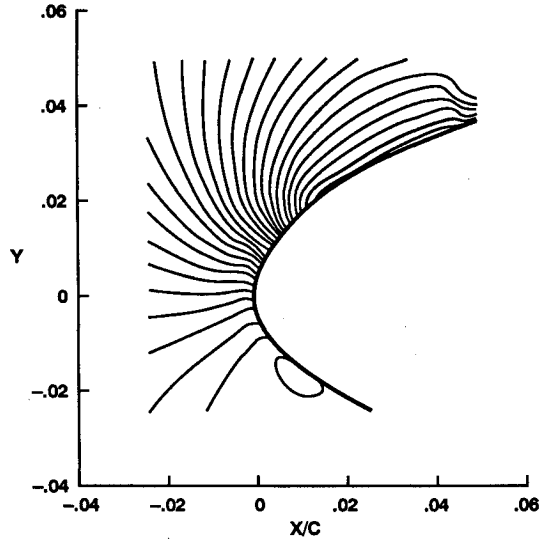

Fig. 7 Fringe contours near the leading edge of an NACA 0012 airfoil at $M_\infty = 0.30$, $\alpha = 10.0$ deg, $k = 0.0$.

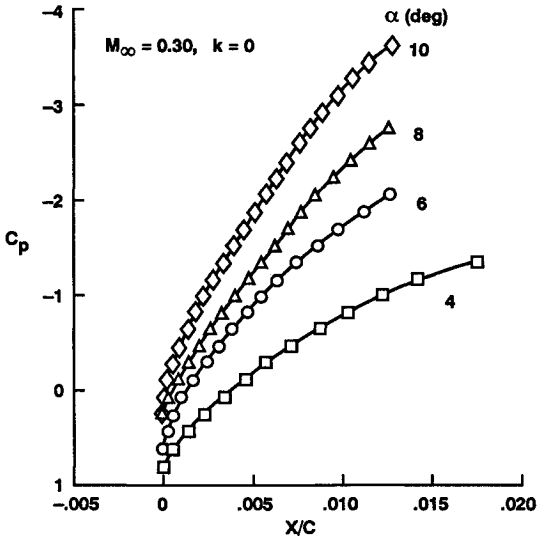

Fig. 8 Steady flow pressure distributions for NACA 0012 airfoil as determined from PDI images, $M_\infty = 0.30$, $k = 0.0$.

grams were digitally processed, and the leading-edge region was greatly enlarged. Three registration markers were placed on one of the rotating tunnel windows that support the airfoil so that a proper orientation and scaling of the fringe patterns could be accomplished. Two triangular markers were arranged below the airfoils so that the distance between the vertical faces was exactly 20% chord; the horizontal surfaces of these triangles were placed so that a line connecting these surfaces was parallel to the airfoil chord, and 10% below the centerline of the airfoil. The triangle above the airfoil was placed so that its lower surface was 20% chord from the top surface of the triangle located below the airfoil. The line connecting the vertical surfaces of these two triangles was perpendicular to the chord at the 25% chord location.

Each interferogram was digitally scanned, and scaled to a selected size by use of these registration markers. A grid was superimposed on the digitized image, and the grid block containing the leading-edge region was selected for further enlargement. This image was then processed using an adaptive contrast-enhancement procedure specially developed for this purpose. This procedure subdivided the region before applying the enhancement, and then locally optimized the contrast. The locally optimized contrast in each subregion was then smoothly matched to the adjoining regions, resulting in a greatly improved interferogram for digital fringe mapping. A photograph of the airfoil was obtained under no-flow conditions, with the PDI plate removed. This no-flow airfoil image was digitized, scaled, and then superimposed on the digitized image of the interferogram, and the combined digital image was used for further analysis. The combined image was mapped using a specially designed, screen-oriented digitizing program that interactively permitted tracing of the various fringes by movement of the cursor via a computer mouse. The stored data was then processed using a least-square-fit, curve-fitting routine. A sample of the resultant fringe contour maps can be seen in Fig. 7.

C. Instantaneous Pressure Distributions

Each fringe in an interferogram is a line of constant density, and by use of the procedure outlined in Sec. V.A., denotes a constant Mach number. Therefore, the fringe maps described above can be used to quantify the effect of unsteadiness on the local pressure distributions of the oscillating airfoil studied in the present experiments. Figure 8 presents pressure distributions near the leading edge of the airfoil for four steady angles of attack at $M_\infty = 0.30$. These plots are obtained by mapping the x location of the intersection of each fringe with the airfoil surface. The fringe numbers are then

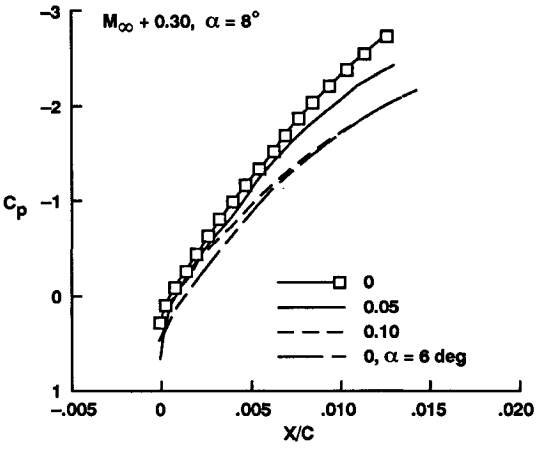

Fig. 9 Comparison of leading-edge pressure distributions in steady and unsteady flows on NACA 0012 airfoil, $M_\infty = 0.30$, $\alpha = 8.0$ deg.

converted to C_p, and the pressure distributions calculated. In each case shown, the distributions are mapped up to the point where the last fringe intersects the surface before the laminar separation bubble occurs, and thus show the pressure distribution associated with the laminar bubble formation (except for $\alpha = 4$ deg, where the bubble was not present).

Figure 9 presents the pressure distributions at $k = 0.05$ and 0.10 at $\alpha = 8$ deg. The pressure distributions for steady flow at $\alpha = 6$ and 8 deg are included for comparison. The curves for $k = 0.05$, and 0.10 are flatter and therefore show progressively lower gradients. The pressure distribution for $k = 0.10$, at $\alpha = 8$ deg is virtually identical to the distribution for $k = 0.0$, $\alpha = 6$ deg, showing that unsteadiness has indeed reduced the instantaneous local pressure gradients.

Figure 10 presents the maximum (suction) C_p value as a function of the angle of attack at $M_\infty = 0.30$, $k = 0.075$. The maximum C_p was determined by counting the fringes through the stall vortex and tracing them back to the leading edge; in the attached flow near the leading edge, any particular fringe can be assigned a C_p value using isentropic flow relations. This plot shows that suction steadily develops over the airfoil as the angle of attack increases. At $\alpha = 12.5$ deg, the C_p has reached a value $= -4.7$, and remains at this level until $\alpha = 13.2$ deg, where it starts decreasing. It is believed that the dynamic stall process begins at $\alpha = 12.5$ deg in this case; during the vortex formation the suction peak remains constant. However, once the vortex begins to convect, the suction peak drops. It is interesting that even though the suction peak

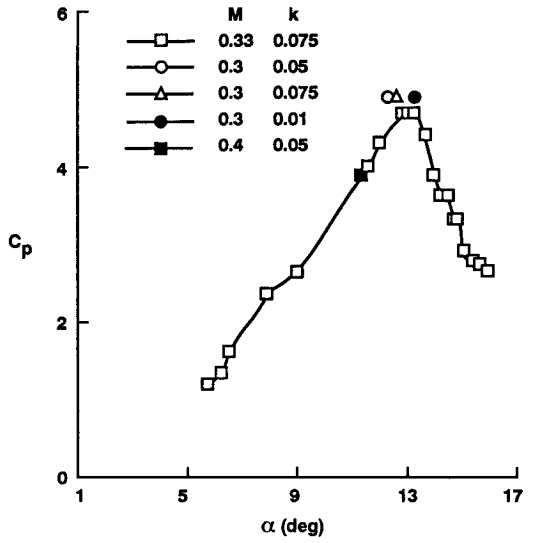

Fig. 10 Variation of minimum suction pressure with change in angle of attack.

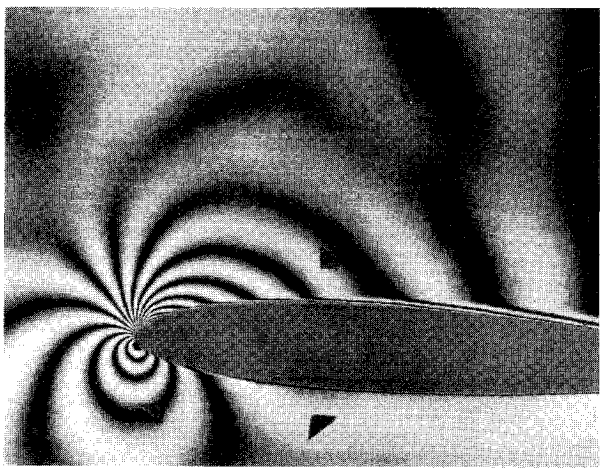

Fig. 11 PDI image of the flowfield for $\alpha = 5.0$ deg, $k = 0.0$, $M_\infty = 0.30$.

drops, there is a substantial suction present over the airfoil as the vortex grows; this increased extent of the low-pressure region enables generation of higher lift until the vorticity leaves the airfoil.

D. Comparison to Prior Experiments

Detailed analysis of the interferograms obtained in the present experiment show that the flow only attains a local Mach number of 0.83 during oscillation at $k = 0.05$, $M_\infty = 0.30$, $\alpha = 10$ deg $-$ sin ωt, even though in earlier dynamic stall experiments[4] surface pressures suggested local Mach numbers as high as 1.3. The two experiments are similar in many respects: both were run at $M_\infty = 0.30$; both performed for $\alpha = 10$ deg $-$ 10 deg sin ωt; both tests were on the NACA 0012 airfoil. However, the present tests were performed at a chord Reynolds number of 6×10^5, whereas the previous tests were performed at $Re = 4 \times 10^6$. A review of the data from the earlier experiments[4] shows that the NACA 0012 airfoil at $M = 0.30$, $k = 0.05$, $\alpha = 10$ deg $-$ 10 deg sin ωt reached a local Mach number of 1.22 at an $\alpha = 13.9$ deg, at which point the leading-edge suction peak was lost, and the dynamic stall process began. The present experiments for the same test conditions show dynamic stall to begin at $\alpha = 12.0$ deg, with a maximum local Mach number of 0.83.

This change in stall behavior, and the decrease in maximum suction that is observed in the present experiment, can be better understood by study of two steady flow conditions: α

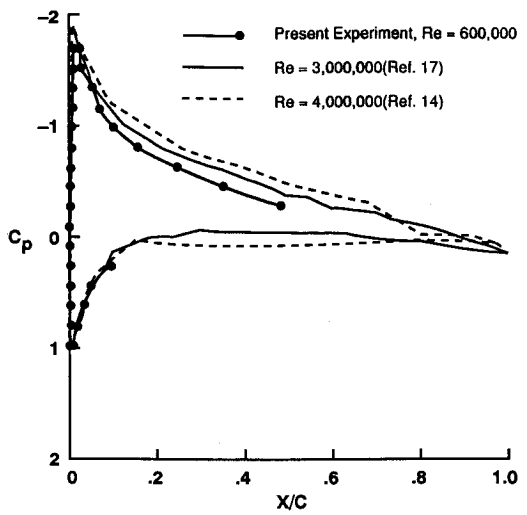

Fig. 12 Comparison of airfoil pressure distributions obtained from different experiments, $\alpha = 5.0$ deg, $M_\infty = 0.30$, $k = 0.0$.

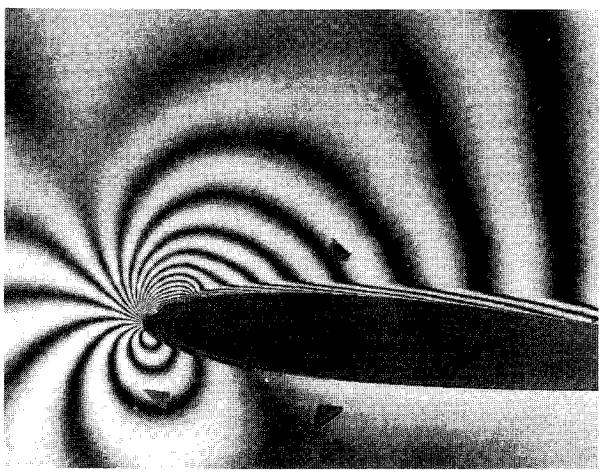

Fig. 13 PDI image of the flowfield for $\alpha = 8.0$ deg, $k = 0.0$, $M_\infty = 0.30$.

$= 5$ and 8 deg, for steady flow at $M_\infty = 0.30$. In Fig. 11, the point-diffraction interferogram for $\alpha = 5$ deg, steady flow, $M_\infty = 0.30$ is presented. This image shows the flow when the laminar separation bubble is not present. The corresponding pressure distribution, determined using the technique outlined above, is compared to two other experiments performed at the same freestream Mach number in Fig. 12. As can be seen in Fig. 12, the present results compare favorably with the referenced experiments, which were performed at significantly higher Reynolds numbers (3.0×10^6 for Ref. 4, and 3.86×10^6 for Ref. 17), especially when the accuracy of $\pm\frac{1}{2}$ fringe is included in the present results.

Figure 13 shows the density field for $\alpha = 8$ deg, for steady flow at $M_\infty = 0.30$, obtained from the present experiment. Here, the flow near the leading edge of the airfoil is quite different. The pressure distribution determined from this interferogram is shown in Fig. 14, again compared to previous experiments. The maximum suction seen in this figure is approximately -2.73, and a plateau appears following the suction peak, extending from $0.015 \leq x/c \leq 0.05$ (the length of the bubble). The maximum C_p observed in this figure is significantly less than that obtained by surface-mounted instantaneous pressure transducers in the two earlier experiments, as shown in the figure.

A laminar separation bubble was observed in the earlier tests,[4] where it appeared as an abrupt change in skin-friction magnitude and frequency content. However, it was only of secondary importance in its influence on the pressure distributions, and appeared as a small, localized perturbation in

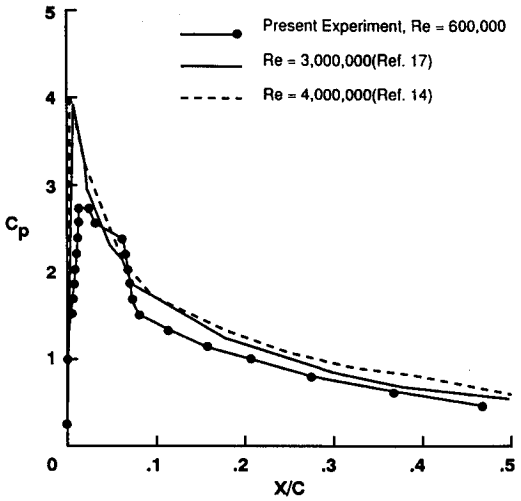

Fig. 14 Comparison of airfoil pressure distributions obtained from different experiments, $\alpha = 8.0$ deg, $M_\infty = 0.30$, $k = 0.0$.

the pressure traces. The effect of the bubble was determined to be secondary at this Reynolds number, since the leading-edge suction remained high well after the laminar separation bubble was detected, and the loss of suction peak appeared at the leading edge, well ahead of the laminar bubble.

However, in the present case, the bubble plays a much more dominant role in modifying the pressure distribution. It is possible that since this bubble is proportionally larger than in the previous test,[4] its influence on the surrounding flowfield is the source of the drop in maximum Mach number that has been observed throughout this set of experiments. The bubble remains a major factor throughout the dynamic stall development in the present experiments. In fact, changes in the bubble behavior seem to be the first indicator that the dynamic stall process has begun. The bubble appears at angles of 6 deg and above, for a wide range of frequencies and Mach numbers. Although its appearance is delayed by oscillation to $\alpha = 8$ deg, its shape and length are essentially unaffected by frequency or Mach number until the separation process begins; the bubble remains intact up to the dynamic stall angle. Thus, the laminar separation bubble is the source of the many differences that are observed in the present lower Reynolds number experiments at high angle of attack.

VI. Concluding Remarks

1) Point diffraction interferometry has permitted detailed study of the complex unsteady flow near the leading edge of an oscillating airfoil, and quantitative flow information has been obtained both on the surface and in the surrounding flowfield for a range of frequencies and Mach numbers.

2) A laminar separation bubble is observed in most of the higher angle conditions, although the occurrence of the bubble can be delayed by unsteadiness.

3) Locally supersonic flow was observed near the leading edge, but the region of supersonic flow is quite small.

4) Digitization of the interferograms has permitted detailed mapping of the instantaneous pressure distribution near the leading edge, and has shown that unsteadiness significantly relieves the pressure gradients that occur in this region.

Acknowledgments

The project was supported by AFOSR-ISSA-89-0067 and AFOSR-MIPR-90-0012 (monitored by L. Sakell and D. Fant), with additional support from NAVAIR (T. Momiyama) and ARO MIPR-ARO-132-90 (T. L. Doligalski). We wish to thank Christopher Boswell of Sterling Federal Systems, for his aid in digitizing the interferograms. The assistance from the staff of the NASA Fluid Mechanics Laboratory is greatly appreciated.

References

[1]Carr, L. W., "Progress in Analysis and Prediction of Dynamic Stall," *Journal of Aircraft*, Vol. 25, No. 1, 1988, pp. 6–17.

[2]Chandrasekhara, M. S., and Carr, L. W., "Flow Visualization Studies of the Mach Number Effects on Dynamic Stall of an Oscillating Airfoil," *Journal of Aircraft*, Vol. 27, No. 6, 1990, pp. 516–522.

[3]Carr, L. W., Platzer, M. F., Chandrasekhara, M. S., and Ekaterinaris, J., "Experimental and Computational Studies of Dynamic Stall," *Numerical and Physical Aspects of Aerodynamic Flows IV*, Springer-Verlag, New York, 1990, pp. 239–258.

[4]McCroskey, W. J., McAlister, K. W., Carr, L. W., and Pucci, S. L., "An Experimental Study of Dynamic Stall on Advanced Airfoil Sections," Vol. 1; "Summary of the Experiment," Vol. 2; "Pressure and Force Data," Vol. 3; "Hot-Wire and Hot-Film Measurements," NASA TM-84245, July 1982.

[5]Lorber, P. F., and Carta, F. O., "Airfoil Dynamic Stall at Constant Pitch Rate and High Reynolds Number," *Journal of Aircraft*, Vol. 25, No. 6, 1988, pp. 548–556.

[6]Carr, L. W., and Chandrasekhara, M. S., "Design and Development of a Compressible Dynamic Stall Facility," *Journal of Aircraft*, Vol. 29, No. 3, 1992, pp. 314–318.

[7]Smartt, R. N., "Point-Diffraction Interferometry as a Diagnostic Tool for Alignment," *Optical Alignment II*, Society of Photo-Optical Instrumentation Engineers, SPIE Vol. 483, 1984.

[8]Bachalo, W. D., and Houser, M. J., "Evaluation and Application of a New Interferometric Technique for Compressible Flow Research," NASA CR-177467, Oct. 1988.

[9]Anderson, R. C., and Milton, J. E., "A Large Aperture Inexpensive Interferometer for Routine Flow Measurements," *ICIASF '89 Record*, Inst. of Electrical and Electronics Engineers, IEEE Publication 89-CH-2762-3, pp. 394–399.

[10]Carr, L. W., Chandrasekhara, M. S., Brock, N. J., and Ahmed, S., "A Study of Dynamic Stall Using Real-Time Interferometry," AIAA Paper 91-0007, Jan. 1991.

[11]Brock, N. J., Chandrasekhara, M. S., and Carr, L. W., "A Real Time Interferometry System for Unsteady Flow Measurements," *ICIASF '91 Record*, Inst. of Electrical and Electronics Engineers, IEEE Publication 91-CH-3038-8, pp. 423–430.

[12]Chandrasekhara, M. S., and Van Dyken, R. D., "Oscillating Airfoil Velocity Field During Large Amplitude Dynamic Stall," *Proceedings of the 8th Symposium on Turbulent Shear Flow*, Technical Univ. of Munich, Munich, Germany, 1991, pp. i-3.1–3.2.

[13]Chandrasekhara, M. S., and Ahmed, S., "Velocity and Vorticity Distributions over an Oscillating Airfoil Under Compressible Dynamic Stall," *AIAA Journal*, Vol. 31, No. 6, 1993, pp. 995, 996.

[14]Duncan, N. J., Thom, A. S., and Young, A. D., "Dynamics of Compressible Fluids," *Mechanics of Fluids*, 2nd ed., Edward Arnold Pub. Ltd., London, 1972, pp. 459–531, Chap. 9.

[15]Van Dyke, M., "An Album of Fluid Motion," Parabolic Press, Stanford, CA, 1982.

[16]Goldstein, R. J., "Optical Systems for Flow Measurement: Shadowgraph, Schlieren, and Interferometric Techniques," *Fluid Mechanics Measurements*, Hemisphere, New York, 1985, pp. 377–422, Chap. 8.

[17]Harris, C. D., "Two-Dimensional Aerodynamic Characteristics of the NACA 0012 Airfoil in the Langley 3-Foot Transonic Pressure Tunnel," NASA TM 81927, April 1981.